Journal of Oceanography, Vol. 63, pp. 267 to 280, 2007

Algorithm and Validation of Sea Surface Temperature Observation Using MODIS Sensors aboard Terra and Aqua in the Western North Pacific

KOHTARO HOSODA[1]*, HIROSHI MURAKAMI[1], FUTOKI SAKAIDA[2] and HIROSHI KAWAMURA[2]

[1]*Earth Observation Research Center, Japan Aerospace Exploration Agency, Sengen, Tsukuba, Ibaraki 305-8505, Japan*
[2]*Center for Atmospheric and Oceanic Studies, Graduate School of Science, Tohoku University, Aoba, Sendai 980-8578, Japan*

(Received 17 June 2006; in revised form 7 November 2006; accepted 11 November 2006)

A regional algorithm to estimate SST fields in the western North Pacific, where small oceanographic disturbance are often found, has been developed using Moderate Resolution Imaging Spectroradiometers (MODIS) aboard Terra and Aqua. Its associated algorithm, which includes cloud screening and SST estimation, is based on an algorithm for the Global Imager (GLI) aboard Advanced Earth Observing Satellite-II (ADEOS-II) and is tuned for MODIS sensors. For atmospheric correction, we compare Multi-Channel SST (MCSST), Nonlinear SST (NLSST), Water Vapor SST (WVSST) and Quadratic SST (QDSST) techniques. For NLSST, four first-guess SSTs are investigated, including the values for MCSST, climatology with two different spatial resolutions, and near-real-time objective analysis. The results show that the NLSST method using high-resolution climatological SST as a first-guess has both good quality and high efficiency. The differences of root-mean-square error (RMSE) between the NLSST models using low-resolution climatology and those using high-resolution climatology are up to 0.25 K. RMSEs of the new algorithm are 0.70 K/0.65 K for daytime (Aqua/Terra) and 0.65 K/0.66 K for nighttime, respectively. Diurnal warming and the stratification of the ocean surface layer under low wind are discussed.

Keywords:
· Infrared SST,
· satellite observation.

1. Introduction

Sea surface temperature (SST) is one of the most important parameters in oceanography and marine meteorology. The SST fields are used as boundary conditions for atmospheric and oceanic models, as well as for the verification of model outputs. High-resolution SST maps can depict oceanic surface currents and eddies. Near-real-time (NRT) processing of SST estimation is therefore sought for fishery and weather forecasting applications. The major advantage of satellite remote sensing of SST is its wide coverage of data acquisition in near-real-time.

Satellite remote sensing to retrieve SST using infrared sensors has been performed for many years using the Advanced Very High Resolution Radiometer (AVHRR) aboard NOAA (National Oceanic and Atmospheric Administration) satellites, the Ocean Color and Temperature Scanner (OCTS) on the Advanced Earth Observing Satellite (ADEOS; Sakaida *et al*., 1998), the Moderate Resolution Imaging Spectroradiometer (MODIS) on the National Aeronautics and Space Administration (NASA) Earth Observing System (EOS) platforms (Brown and Minnett, 1999), and Global Imager (GLI) on the Advanced Earth Observing Satellite-II (ADEOS-II; Sakaida *et al*., 2006a). After MODIS sensors were launched on 18 December 1999 (Terra) and 4 May 2002 (Aqua), global observation has been continued to the present. The specified requirements for noise equivalent temperature difference (NEdT) of MODIS thermal infrared bands for SST retrieval is 0.05 K, which is a considerable improvement over that of AVHRR (NEdT = 0.12 K; Goodrum *et al*., 2000). Early on-orbit observations of MODIS (Wan, 2002) showed that the standard deviation of the MODIS 11 μm band, which is used mainly for SST estimation, is no greater than 0.05 K at sub-area sites where surface and atmospheric conditions are assumed to be uniform. In addition, plentiful bands observed by MODIS yield more accurate atmospheric correction and cloud screening. It

* Corresponding author. E-mail: hosoda.kohtaroh@jaxa.jp

is therefore anticipated that clear SST fields are obtained from MODIS sensors.

Using infrared radiometers, SSTs are estimated with high resolution (about 1 km) only under cloud-free conditions. Cloud-screening algorithms for each sensor should be developed carefully to avoid cloud contamination of the dataset. The atmospheric absorption of radiation between the sea surface and the satellites, primarily by water vapor, is corrected by brightness temperature differences (BTDs) at a few spectral bands. McClain *et al*. (1985) introduced the Multi-Channel SST (MCSST) algorithm, which presumes a linear relation between BTDs and the total amount of water vapor. To account for a nonlinear relationship in the effect of water vapor and BTDs, Emery *et al*. (1994) developed Water Vapor SST (WVSST) and Quadratic SST (QDSST). Walton (1988) and Walton *et al*. (1998) suggested Cross Product SST (CPSST) and Nonlinear SST (NLSST) methods.

Sobrino *et al*. (1993) pointed out that global versions of SST estimation are inadequate to represent all atmospheric variation between tropical and polar regions, and suggested that regional algorithms would not pose such a problem. Sakaida and Kawamura (1992) and Shenoi (1999) showed that the use of regional SST retrieval algorithms from AVHRR/NOAA observations has lower root-mean-square error (RMSE) than the respective global algorithms in the western North Pacific and northern Indian Oceans. The MODIS SSTs processed at the Japan Aerospace Exploration Agency/Earth Observation Research Center (JAXA/EORC) are expected to be more accurate than those estimated from the global algorithm for MODIS (Brown and Minnett, 1999) because they are retrieved from a regional SST algorithm that is adjusted to the western North Pacific region.

Our purpose is to describe the development and validation of the MODIS SST algorithm processed at JAXA/EORC. Section 2 provides informations on the data used in this study. Section 3 describes details of the algorithm, including cloud detection and atmospheric correction. We compare four atmospheric correction models for MODIS data and validate each model using drifting-buoy observation as sea-truth in Section 4. A better atmospheric correction model for MODIS SST at JAXA/EORC and remaining problems are discussed in Section 5. Finally, we present a summary of the results of this study in Section 6.

2. Data

Two sun-synchronous satellites, Terra and Aqua, carry MODIS, which are visible and infrared radiometers. The satellites are 705 km from the Earth's surface and ±55° scanning covers a 2330 km swath, thereby providing global coverage. Terra has a descending pass in the morning (10:30 AM), while Aqua has an ascending pass

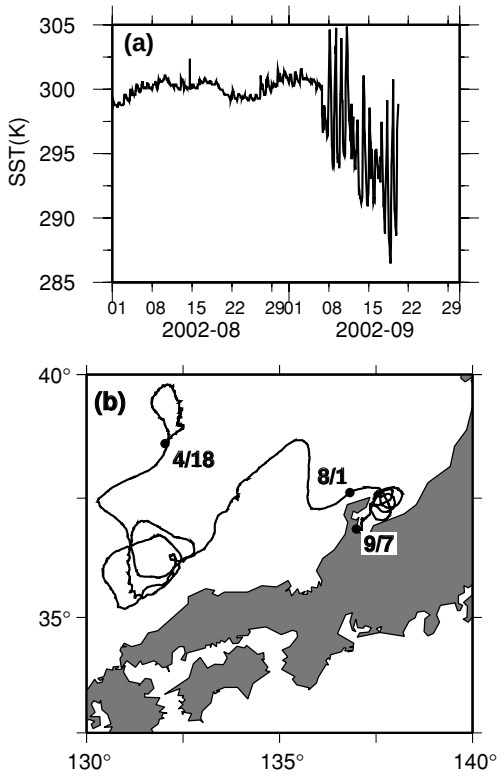

Fig. 1. (a): Time series of buoy SST for drifting buoy No. 21531. (b): Trajectory of drift buoy No. 21531, which ran aground. Black points indicate the positions of buoy on associated days.

in the afternoon (1:30 PM). In all, MODIS has 36 spectral bands ranging from 0.4–14.4 μm. Two bands are imaged at a resolution of 250 m at nadir, with five bands at 500 m; the resolution of the remaining 29 bands is 1 km. To retrieve SST, bands with spatial resolution of 1 km are used.

At JAXA/EORC, ocean products around Japan derived from MODIS are processed in near-real-time and are accessible via the Internet. The images and data with acquisition time (UTC time in minutes) are available within a few hours of their observation. The ground stations for receiving MODIS data are Tokai University Space Information Center (TSIC; 32.8°N, 130.9°E, from April 2001) and the JAXA/Earth Observation Center (EOC; 36.0°N, 139.3°E, from August 2004).

The algorithm for retrieving near-real-time SST from MODIS in JAXA/EORC is based on that for Global Imager (GLI) on the Advanced Earth Observing Satellite-II (ADEOS-II: Sakaida *et al*., 2006a). Coefficients for cloud detection and atmospheric correction are tuned using MODIS Level 1B data and collocated buoy bulk SST observations collected in the western North Pacific region (see Section 3). This algorithm and its associated

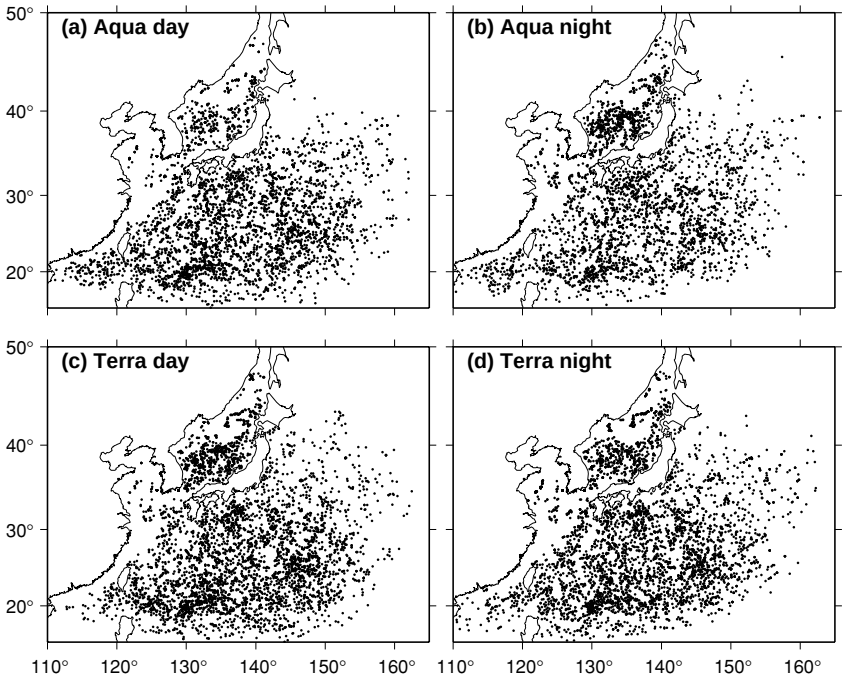

Fig. 2. Latitude-longitude location of match-up (MODIS to buoy observation) data points. Data acquisition period is 2002–2004.

data are referred to hereafter as "MODIS NRT SST".

Processing of the version 1 MODIS NRT SST in JAXA/EORC began in April 2001 (Murakami, 2002). The version 2 algorithm (Hosoda, 2004) was used to produce MODIS NRT SST during 5 October 2004–30 September 2005; the version 3 algorithm has been applied since 1 October 2005. In versions 1 and 2, the Multi-Channel SST (MCSST) method was employed for atmospheric attenuation correction. The version 1 algorithm was based on a radiative transfer model. During development of the version 2 algorithm, cloud detection schemes were improved based on Level 1B MODIS images (see Subsection 3.1); the MCSST coefficients were derived from match-up data collected in the western North Pacific region (20–50°N, 115–155°E) during February–April, 2004. When developing the version 3 algorithm, match-up data were collected during January 2002–December 2003 in the western North Pacific region, and the atmospheric correction method was changed from MCSST to that of the nonlinear SST (NLSST) (Walton *et al*., 1998). The NLSST method was adopted after the results of algorithms were validated against buoy observations, as described in Sections 4 and 5.

Sea-truth data for deriving match-ups represent the "bulk SST" observed by drifting buoys within the uppermost 1 m layer of the ocean. A quality control procedure is required for buoy data in order to reject anomalous data, which can result from accidental traction by ships and landing of the buoy. To reject suspicious buoy data, we used two tests applied to a time-series of each buoy. First, buoy data are excluded from making match-ups if the duration of buoy observation is less than 3 days. The next test examines the short-term variation of buoy SST. We eliminated buoy data with a magnitude of diurnal variation (maximum–minimum) of SST larger than 8 K. Figure 1 portrays an example of the time-series of SST and trajectory of a buoy (buoy ID: 21531) suspected of grounding. In August 2002, the buoy ran into Toyama Bay, Japan, and started to circle counterclockwise. The diurnal variability within this time was less than 3 K. After 7 September, the buoy motion was negligible and the diurnal variations of SST were greater than 8 K. The second quality control test detects and rejects such abnormal data.

Infrared observations by satellite require that the measured area should be cloud free. We used the cloud-detection algorithm using the brightness temperatures and reflectances of satellite observations (Subsection 3.1). During development of the algorithm (Subsection 3.2), the clear-ratio around the buoy observation, which is defined as the fraction of clear pixels of MODIS within an 11×11-pixel array, is set to be greater than 95% to avoid cloud contamination. In addition, we used initial-guess satellite SSTs derived from the version 2 MODIS NRT SST algorithm. Residuals between the *in situ* and the initial-guess SST that are greater than 4 K are eliminated from determination of the SST retrieval equations in or-

Table 1. Cloud detection tests for the MODIS NRT algorithm. Schemes denoted by "Y" are used in each test: Scheme-1, day and outside sun-glitter region, Scheme-2, day and inside sun-glitter region, Scheme-3, night; ϕ, latitude (degree), θ_r, reflection angle (degree); R_λ, reflectance of λ μm band (%); BT_λ, brightness temperature of λ μm band (K); ∇_{mv}, difference between the maximum and the center of a 3×3-pixel array; ∇_{nv}, difference between the center and the minimum of a 3×3-pixel array; ∇_{mn}, maximum-minimum difference in a 3×3-pixel array.

Group		Cloud detection test	Scheme		
			1	2	3
Gross test	(1)	$BT_{11} < \mathrm{Max}(-0.0175\phi^2 + 293, 269.15)$	Y	Y	Y
Reflectance test	(2)	$R_{0.865}/R_{0.470} > 1.475 - 0.037\theta_r$	N	Y	N
	(3)	$R_{0.865}/R_{0.470} > 0.55$	Y	N	N
	(4)	$R_{1.240}/R_{0.470} > 1.442 - 0.0375\theta_r$	N	Y	N
	(5)	$R_{1.240}/R_{0.470} > 0.58 - 0.003\theta_r$	Y	N	N
	(6)	$R_{1.240} > 60.0 - 2.12\theta_r$	N	Y	N
	(7)	$R_{1.240} > 7$	Y	N	N
BTD test	(8)	$BT_{11} - BT_{12} > \exp(0.08BT_{11} - 23.2) + 1.0$	Y	Y	Y
	(9)	$BT_{11} - BT_{8.6} < 0$	Y	Y	Y
	(10)	$BT_{3.7} - BT_{12} < \exp(0.0342BT_{11} - 9.375) - 1.0$	N	N	Y
	(11)	$BT_{3.7} - 2BT_{11} + BT_{12} > 2$	N	N	Y
	(12)	$BT_{3.7} - 2BT_{11} + BT_{12} < -1$	N	N	Y
Uniformity test	(13)	$\nabla_{mv}BT_{11} > 1.5$ and $\nabla_{mn}(BT_{11} - BT_{12}) > 2.5$	Y	Y	Y
	(14)	$\nabla_{nv}R_{1.240} > 2.5$	Y	Y	N
	(15)	$\nabla_{mv}BT_{3.7} > 2.5$	N	N	Y

der to avoid anomalous buoy data or cloud contamination in satellite observations.

The atmospheric correction model is developed through regression analyses using match-ups observed in 2002 and 2003 (Subsection 3.2). The derived models are validated using match-up data observed during 2002–2004 (Section 4). Validations of the algorithms are performed using the match-up data with a clear-ratio greater than 90%. The temporal differences between the *in situ* and satellite observations are less than 3 hours.

Figure 2 shows spatial distributions of match-up data collected during 2002–2004. Drifting buoys rarely run into coastal regions such as the eastern coast off the China and the Yellow Sea. So the match-ups are mainly distributed in the open ocean.

3. Algorithms of Cloud Detection and Atmospheric Correction

3.1 Cloud detection

Cloud-detection in the MODIS NRT SST algorithm is implemented using several threshold tests for identifying a pixel as cloud-free. The threshold tests for cloud detection are based on those for ADEOS-II/GLI algorithm (Sakaida *et al*., 2006a). Table 1 shows cloud detection tests used in the MODIS NRT SST algorithm (ver. 2 and 3). We use the term "scheme" to signify the combination of cloud detection tests. Scheme-3 (nighttime) cloud detection algorithms are used when the solar zenith angle θ_{suz} is greater than 86.5°. In daytime, the scheme-2 algorithm is used in sun-glitter regions, and the scheme-1 algorithm outside these regions. According to Sakaida *et al*. (2000), the sun-glitter region is specified by the reflection angle θ_r, which is calculated from

$$\cos\theta_r = \frac{\cos\theta_{suz} + \cos\theta_{saz}}{2\cos\omega}, \tag{1}$$

where θ_{saz} is the satellite zenith angle. The angle ω can be derived from the relation

$$\cos 2\omega = \cos\theta_{saz}\cos\theta_{suz} + \sin\theta_{suz}\sin\theta_{saz}\cos(\phi_{sua} - \phi_{saa}), \tag{2}$$

where ϕ_{sua} and ϕ_{saa} respectively denote the azimuthal angles of the sun and satellite. The limit angle for θ_r to specify the sun-glitter region is 25 degrees, as determined empirically from MODIS data.

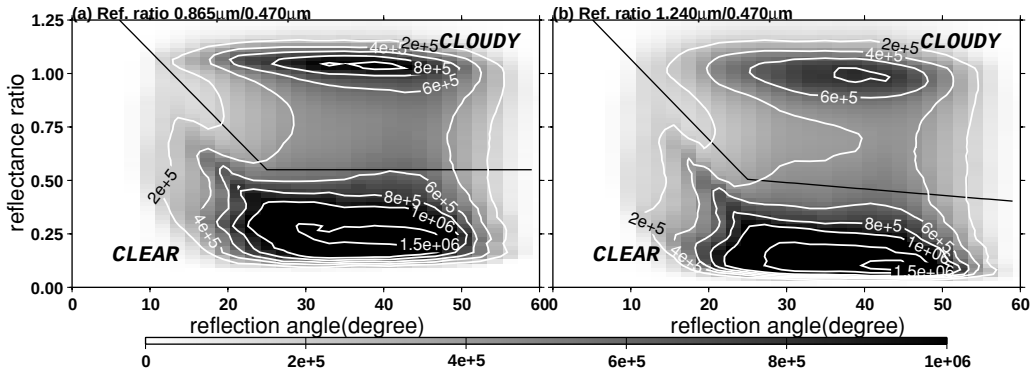

Fig. 3. Frequency diagrams of pixels on the domain of $R_{0.865}/R_{0.470}$ (a) and $R_{1.240}/R_{0.470}$ (b) vs. reflection angle. Shade and contours indicate the frequency values. Thick black lines show the cloud detection thresholds: (a) Eqs. (2) and (3) in Table 1, (b) Eqs. (4) and (5) in Table 1, respectively.

Cloud detection tests are categorized according to four groups. The first group is a gross test (Table 1, (1)), which determines cloudy pixels if the brightness temperature at 11 μm is less than a threshold value, which is defined as a quadratic function of latitude (Tanahashi *et al*., 2000).

The second group (Table 1, (2)–(7)) uses visible and near-infrared reflectance (R_λ, where λ is central wavelength (μm) of each band). It is widely known that the ratio of reflectance in two different bands is an effective means in detecting clouds in daytime. Reflections of the solar irradiance at the cloud top have no strong wavelength dependency. Therefore, a reflectance ratio near 1.0 indicates that the pixel is cloudy. Ackerman *et al*. (1997) showed that the reflectance difference in wavelength above and below 0.72 μm is useful for identifying clouds. Sakaida *et al*. (2006a) pointed out that the reflectance ratio of $R_{0.865}$ and $R_{0.545}$ performs better in detecting clouds. From MODIS L1B data, it is inferred that reflectance ratios using $R_{0.470}$ are more effective for detecting clouds than those using $R_{0.545}$, since the former ratios for the ocean surface in the sun-glitter region are low enough to be distinguishable from cloudy pixels. Figure 3 shows frequency diagrams of $R_{1.240}/R_{0.470}$ and $R_{0.865}/R_{0.470}$ as a function of the reflection angle (θ_r) from MODIS L1B data. In order to the possibility of masking clear pixels in a sun-glitter region, the linear threshold function and sun-glitter region ($\theta_r < 25°$) are defined empirically (Table 1, (2)–(5)). To compensate the reflectance ratio test, only tests using 1.24 μm (Table 1, (6) and (7)) are added.

The third group (Table 1, (8)–(12)) consists of BTD tests. The test using BTD between 11 μm and 12 μm is known as a split window method, which is useful for detecting relatively thin clouds. It has been pointed out that BTD under clear conditions depends on the brightness temperature at 11 μm, BT_{11}, where BT_λ denotes a brightness temperature at wavelength λ μm. The threshold function for GLI (Sakaida *et al*., 2006a) is determined as an exponential function of BT_{11}. For cloud detection used in the MODIS NRT SST algorithm, the coefficients in the exponential function are adjusted from MODIS L1B data (Table 1, (8)). A test using BTD between 8.6 μm and 11 μm (Table 1, (9)) is also useful for detecting clouds (Strabala *et al*., 1994). Since the BTD is only weakly dependent on the BT_{11}, the threshold for this test is defined as a constant value. For nighttime observation, BTDs between 3.7 μm and other bands are used as cloud detection tests (Table 1, (10)–(12)). Stowe *et al*. (1999) used a BTD between 3.7 μm and 12 μm with a threshold function of BT_{11} for nighttime tests (Table 1, (10)). Sakaida *et al*. (2000) and Guan *et al*. (2003) used the combination of brightness temperatures at 3.7 μm, 11 μm and 12 μm to detect clouds during nighttime. The coefficients of these tests are adjusted to MODIS data (Table 1, (11) and (12)).

The fourth group (Table 1, (13)–(15)) comprises uniformity tests, which are based on the fact that brightness temperatures and reflectances over clear ocean are more spatially homogeneous than those over cloudy regions. Although these tests are very powerful, their reliability is low in coastal and frontal regions. From the fact that the brightness temperature at a cloudy pixel is lower than that at a clear pixel, uniformity of BT_{11} is evaluated by calculating the difference between the maximum value in a 3×3-pixel box and the center pixel value, as used by Rossow and Garder (1993). In addition, the uniformity of the BTD (BT_{11}–BT_{12}) is ensured to avoid masking the frontal region as a cloud (Table 1, (13)). The uniformities of BTD and reflectance (Table 1, (13) and (14)) are evaluated from the difference between maximum and minimum difference in a 3×3-pixel box. A uniformity test using $BT_{3.7}$ is used only at night (Table 1, (15)), since the solar reflection is contaminated at 3.7 μm in daytime.

Table 2. Coefficients of the SST retrieval equations (Eqs. (3), (4), (5) and (6)) for day observations.

	a_0	a_1	$\alpha_{8.7}$	$\beta_{8.7}$	$\alpha_{8.7}'$	α_{12}	β_{12}	α_{12}'
	Aqua/Day (number of data: 4665)							
MCSST	–12.949	1.056	–1.367	0.498	—	3.062	1.235	—
NLSST-1	2.517	1.002	–0.770	0.416	–0.011	–0.068	1.231	0.110
NLSST-2	–6.983	1.035	–0.538	0.414	–0.024	–0.065	1.337	0.114
NLSST-3	–8.998	1.043	–0.647	0.510	–0.024	0.377	1.223	0.099
NLSST-4	8.836	0.980	–0.671	0.429	–0.011	–0.613	1.210	0.133
QDSST	–16.247	1.069	–1.062	0.543	–0.026	1.479	1.083	0.655
WVSST	–11.438	1.052	–1.438	0.507	0.000	2.991	1.458	0.000
	Terra/Day (number of data: 3129)							
MCSST	–15.855	1.067	–1.237	0.364	—	3.176	1.493	—
NLSST-1	–25.705	1.098	0.095	0.325	–0.044	–0.363	1.592	0.134
NLSST-2	–14.605	1.060	–0.093	0.342	–0.034	–0.580	1.441	0.144
NLSST-3	–15.909	1.064	0.060	0.278	–0.037	–0.455	1.547	0.141
NLSST-4	–17.953	1.071	0.103	0.317	–0.036	–0.345	1.538	0.134
QDSST	–16.068	1.064	0.002	0.455	–0.202	1.890	1.213	0.611

3.2 Atmospheric correction

3.2.1 MCSST

The MCSST equation, which was used in previous versions and is examined in the version 3 development of the MODIS NRT SST algorithm, is based on that for the ADEOS-II/GLI algorithm (Sakaida *et al.*, 2006a). The SST is retrieved from the following equation:

$$MCSST = a_0 + a_1 BT_{11} + \sum_{\lambda=3.7,8.7,12} \alpha_\lambda \overline{BT_{11} - BT_\lambda} + \sum_{\lambda=3.7,8.7,12} \beta_\lambda \overline{BT_{11} - BT_\lambda} \left(\sec\theta_{sza} - 1\right). \quad (3)$$

Overbars on the BTDs signify average values in a 7×7-pixel array. The satellite zenith-angle term corrects for the effects of increased path length at larger zenith angles.

3.2.2 WVSST and QDSST

Emery *et al.* (1994) assumed that the weighting factor α of the MCSST (Eq. (3)) is linearly proportional to the total atmospheric water vapor, and proposed Water Vapor SST (WVSST) and Quadratic SST (QDSST) algorithms for correcting atmospheric attenuation. Based on their models, WVSST and QDSST equations evaluated in this research are

$$WVSST = a_0 + a_1 BT_{11} + \sum_{\lambda=3.7,8.7,12} \left(\alpha_\lambda WV + \alpha_\lambda'\right)\overline{BT_{11} - BT_\lambda} + \sum_{\lambda=3.7,8.7,12} \beta_\lambda \overline{BT_{11} - BT_\lambda} \left(\sec\theta_{sza} - 1\right), \quad (4)$$

$$QDSST = a_0 + a_1 BT_{11} + \sum_{\lambda=3.7,8.7,12} \left(\alpha_\lambda \overline{BT_{11} - BT_\lambda} + \alpha_\lambda'\right)\overline{BT_{11} - BT_\lambda} + \sum_{\lambda=3.7,8.7,12} \beta_\lambda \overline{BT_{11} - BT_\lambda} \left(\sec\theta_{sza} - 1\right), \quad (5)$$

where $WV = W_0/\cos\theta_{sza}$, W_0 is the total-column atmospheric water vapor from the sea surface to the satellite, as estimated from Advanced Microwave Scanning Radiometer for EOS (AMSR-E) on the Aqua. Since Terra has no microwave radiometer for estimating total water vapor, here the WVSST model is evaluated for Aqua MODIS only.

3.2.3 NLSST

Walton *et al.* (1998) developed the Nonlinear SST (NLSST) algorithm, in which the weighting factor α of the MCSST is assumed to be proportional to a first-guess SST value obtained in various ways. The NLSST model evaluated in this study has the following form:

$$NLSST = a_0 + a_1 BT_{11} + \sum_{\lambda=3.7,8.7,12} \left(\alpha_\lambda T_{sfc} + \alpha_\lambda'\right)\overline{BT_{11} - BT_\lambda} + \sum_{\lambda=3.7,8.7,12} \beta_\lambda \overline{BT_{11} - BT_\lambda} \left(\sec\theta_{sza} - 1\right), \quad (6)$$

where T_{sfc} is a first-guess SST value.

The α' terms in Eq. (6) are not part of the original NLSST algorithm (Walton *et al.*, 1998). We include these

Table 3. Coefficients of the SST retrieval equations for night observations.

	a_0	a_1	$\alpha_{3.7}$	$\beta_{3.7}$	$\alpha_{3.7}'$	$\alpha_{8.7}$	$\beta_{8.7}$	$\alpha_{8.7}'$	α_{12}	β_{12}	α_{12}'
	Aqua/Night (number of data: 4521)										
MCSST	−3.469	1.021	−1.107	−0.282	—	−0.224	0.388	—	0.643	0.368	—
NLSST-1	7.311	0.984	−2.102	−0.227	0.042	0.023	0.344	−0.010	−1.643	0.507	0.095
NLSST-2	10.054	0.975	−2.102	−0.198	0.042	0.099	0.320	−0.011	−1.998	0.545	0.108
NLSST-3	6.640	0.986	−1.804	−0.212	0.027	−0.023	0.379	−0.005	−0.922	0.358	0.062
NLSST-4	45.391	0.856	−1.985	−0.029	0.038	−0.816	0.372	0.024	−2.557	0.513	0.120
QDSST	1.855	1.000	−1.164	−0.419	−0.086	0.381	0.683	−0.201	1.186	−0.304	0.123
WVSST	−4.333	1.024	−1.061	0.000	0.000	−0.306	0.160	0.000	0.684	1.266	0.001
	Terra/Night (number of data: 3095)										
MCSST	−6.080	1.027	−0.918	−0.619	—	−0.242	0.449	—	1.272	−0.662	—
NLSST-1	0.110	1.006	−1.889	−0.540	0.045	−0.217	0.434	−0.003	−0.967	−0.467	0.102
NLSST-2	3.533	0.994	−2.031	−0.498	0.050	−0.152	0.412	−0.002	−1.520	−0.394	0.123
NLSST-3	1.027	1.002	−1.133	−0.842	0.022	−0.233	0.488	−0.001	0.573	−1.133	0.057
NLSST-4	4.962	0.987	−1.198	−0.587	0.009	−0.160	0.396	0.007	0.772	−0.599	0.014
QDSST	−5.469	1.023	−1.291	−0.702	−0.172	0.322	0.458	−0.105	0.438	−0.750	0.687

Table 4. Results of SST validation for each atmospheric correction model for developing version 3 MODIS NRT SST (MC, MCSST; NL, NLSST; QD, QDSST; WV, WVSST) along with version 2 and NASA standard product in the region around Japan. Bold typeface and underlined numbers show the best and second-best results for each satellite in daytime/nighttime, respectively.

		MC	NL-1	NL-2	NL-3	NL-4	QD	WV	Ver. 2	NASA
		Aqua (number of data: 7007 (day)/5215 (night))								
Day	Bias	−0.101	0.202	0.242	–0.014	−0.022	**−0.004**	−0.053	−0.242	−0.063
	RMSE	0.771	0.862	0.870	**0.702**	0.725	0.729	0.765	0.792	0.810
Night	Bias	−0.223	−0.191	−0.183	−0.141	–0.121	**−0.050**	−0.163	0.249	−0.245
	RMSE	0.754	0.668	0.669	0.647	0.647	**0.628**	0.673	0.713	0.932
		Terra (number of data: 7490 (day)/5035 (night))								
Day	Bias	−0.065	0.117	0.302	−0.041	–0.040	**0.000**	—	−0.294	−0.240
	RMSE	0.734	0.798	0.909	**0.654**	**0.654**	0.680	—	0.875	0.846
Night	Bias	−0.151	−0.101	−0.096	–0.051	−0.053	**0.004**	—	−0.170	−0.184
	RMSE	0.724	0.669	0.670	**0.660**	0.683	0.664	—	0.760	0.887

terms since the equation should have consistency in its formulation with those of WVSST and QDSST, and since these terms are expected to be applicable for calibration of the first-guess SST.

The first-guess SST is an important issue in the development of NLSST models. We evaluate the following four cases in the next section.

1. MCSST values estimated from Eq. (3) (simultaneous observation, 1 km): NLSST-1.
2. Reynolds climatological SST data (monthly, 1 degree; Reynold and Smith, 1994): NLSST-2.
3. Pathfinder climatological SST data (monthly, 4 km; Kilpatrick *et al.*, 2001): NLSST-3.
4. Near-real-time objective analysis SST data

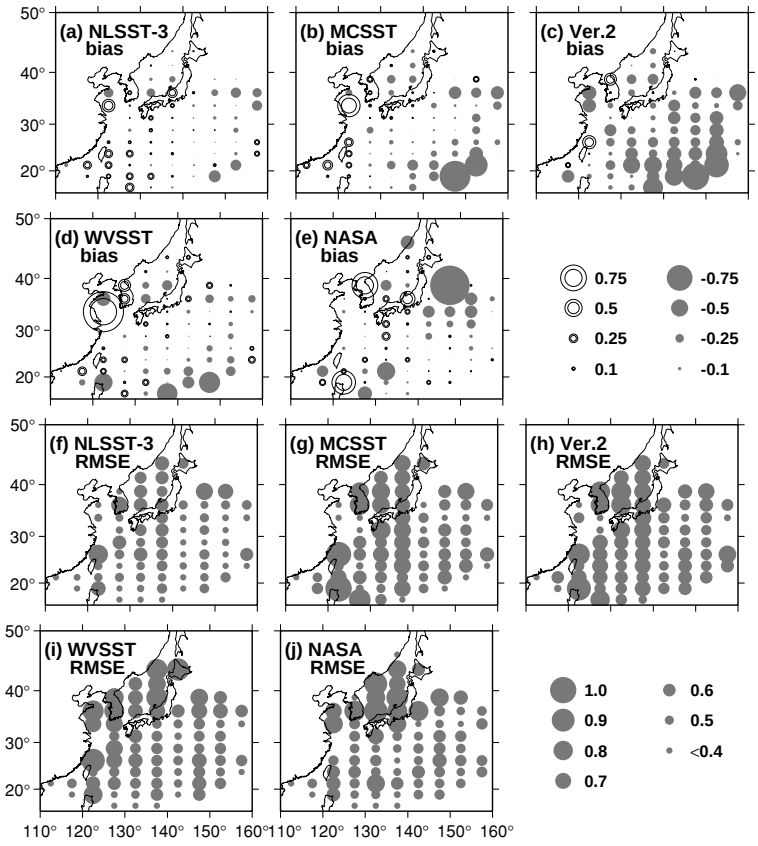

Fig. 4. Spatial distributions of bias and RMSE of Aqua/MODIS daytime SST errors for NLSST-3 (a, f), MCSST (b, g), version 2 SST (c, h), WVSST (d, i) and NASA standard product (e, j). The values are calculated in a 2.5° × 5° (lat. × lon.) box. (a–e): Double circles mean a positive bias; shade circles indicate a negative bias.

(NGSST-O; daily, 5 km; Sakaida *et al*., 2006b): NLSST-4.

3.2.4 Coefficients for each algorithm

As described in Section 2, the number of match-up data samples for development and the coefficients for SST retrieval equations are shown in Tables 2 and 3; the number of match-ups for validation are shown in Table 4.

4. Validation of Atmospheric Correction Models for MODIS SST

Table 4 summarizes validation results of MODIS NRT SST models. Bias is defined as MODIS SST minus buoy SST. For reference, we show the validation results of the version 2 algorithm and the NASA standard product of MODIS SST (4.88 km resolution; Brown and Minnett, 1999, http://podaac.jpl.nasa.gov:2031/DATASET_DOCS/modis_sst.html), using the same match-up dataset collected in the western North Pacific region. Bold typeface and underlined numbers indicate the best and second-best results in each satellite and day/night. Spatial distributions of bias and RMSE of several algorithms for Aqua daytime SST are shown in Fig. 4.

Based on new match-up data, the MCSST algorithm can be marginally improved in the southeast area (negative bias), the Sea of Japan and the Kuroshio recirculation region (large RMSE). Although the NASA standard product has little bias except for the Kuroshio Extension region, the RMSE of the product in the Sea of Japan are as large as 0.9 K. The spatial resolution of the NASA product is a possible source of errors since small oceanographic disturbances with high spatial SST gradient are often found in these region. This argument might be particularly applicable to the results with 1-km resolution, since the errors of the regional algorithm are slightly larger in the Kuroshio and the Sea of Japan regions than those in the open-ocean. Although the regional MCSST algorithm is slightly better than the global dataset, RMSEs of the new MCSST algorithms for Terra and Aqua are greater than 0.7 K. Another algorithm is therefore required for atmospheric correction.

Table 4 shows that most models that include

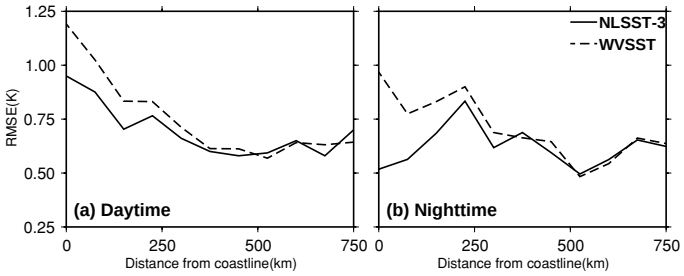

Fig. 5. RMSE of MODIS SST as a function of distance from the coastline. Solid and broken lines denote RMSE functions of NLSST-3 and WVSST, respectively.

nonlinear effects (WVSST, QDSST and NLSST) exhibit better quality than those with MCSST algorithms. Note, however, that the NLSST-1 (T_{sfc}: MCSST) and NLSST-2 (T_{sfc}: Reynolds SST) models in daytime are worse than the MCSST model. Walton *et al*. (1998) pointed out that the MCSST values are not suitable for the first-guess SST in the NLSST model since they might be contaminated by clouds. The NLSST-2 model uses Reynolds climatological SST as a first-guess, whereas the NLSST-3 model also uses climatological SST from the Pathfinder dataset. Since the only difference between these two models is spatial resolution, it should be emphasized that high-resolution data are required for the nonlinear model. It should also be pointed out that the quality of the NLSST-3 is as good as that of the NLSST-4 model, which uses near-real-time SST data as a first-guess.

The WVSST model is no better than the NLSST-3,4 or QDSST. Worse performance would be the result of an estimation error for water vapor in coastal regions, where the microwave measurements are affected by land, as suggested from Fig. 4. This feature is more apparent in Fig. 5, which shows the RMSEs of MODIS NLSST (NLSST-3) and WVSST on Aqua as functions of distance from coastlines. The quality of WVSST is worse than that of NLSST in locations less than 250 km from the coast. In addition to land contamination, the spatial resolution of integrated total water vapor of the atmosphere observed by the AMSR-E instrument is as low as about 25 km. The spatial resolution might also affect the WVSST quality, as suggested by the impact of spatial resolution on the first-guess SST in NLSST models.

Figure 6 shows estimation errors of MODIS SST as a function of buoy SST. Results obtained by the MCSST and QDSST models show biases related to buoy SST. In daytime, a small positive bias is apparent in the middle temperature range (about 290 K), whereas MODIS SST has a small negative bias in the high temperature range (over 300 K). At night the bias shows a negative trend. These relations are weak in the NLSST-3 model, which suggests that the nonlinear effects of water vapor are well-

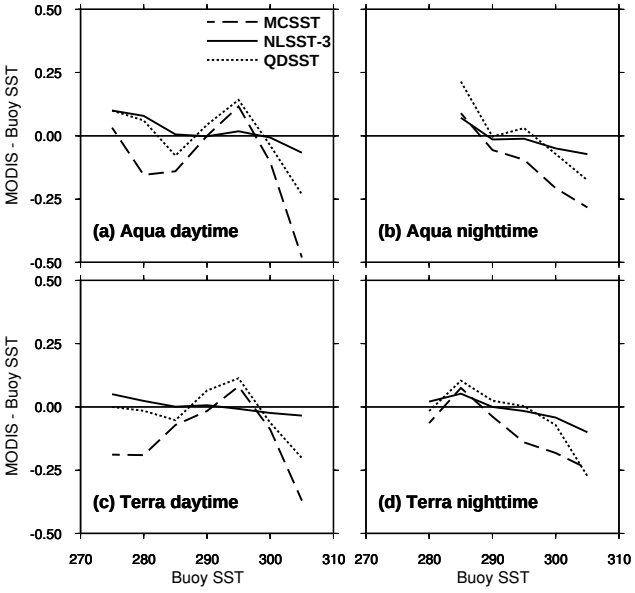

Fig. 6. Differences of MODIS SST and buoy SST as a function of buoy SST. Solid lines denote differences for NLSST-3; broken and dashed lines denote ones for MCSST and QDSST, respectively.

corrected using the first-guess SST.

Temporal variations of estimation errors in MODIS MCSST and NLSST-3 are shown in Fig. 7, in which bias is defined as MODIS-buoy SST. The errors of MCSST models reflect the seasonal variation of biases: a positive bias occurs in winter and a negative one in summer. The RMSEs also fluctuate temporally with large amplitudes. These temporal variations occur notably in daytime SST. The temporal variation at nighttime is not so evident because usage of the 3.7 μm band in atmospheric correction (Eq. (3)) works well. The bias and RMSE of nighttime SSTs show identical fluctuations to those of daytime SSTs (figure not shown) if the 3.7 μm band is not used in atmospheric correction at nighttime. Although the errors

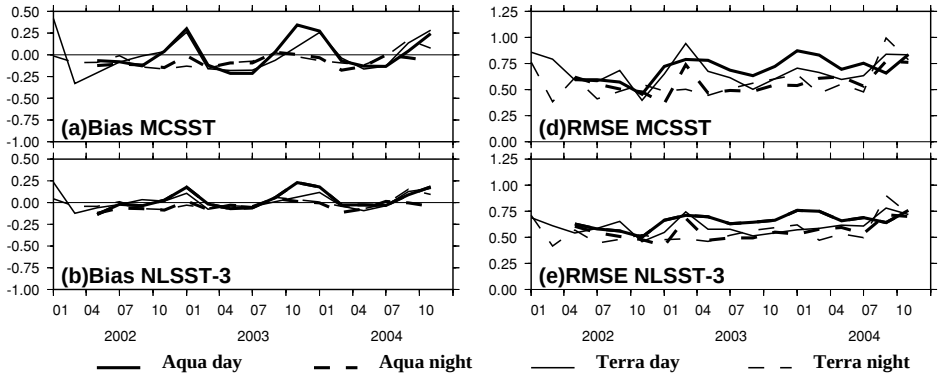

Fig. 7. Time series of MODIS SST quality: (a, b) Bias (defines as MODIS-buoy SST) and (c, d) RMSE. Thick lines (solid/dashed) show Aqua (daytime/nighttime) and thin lines (solid/dashed) show Terra (daytime/nighttime), respectively.

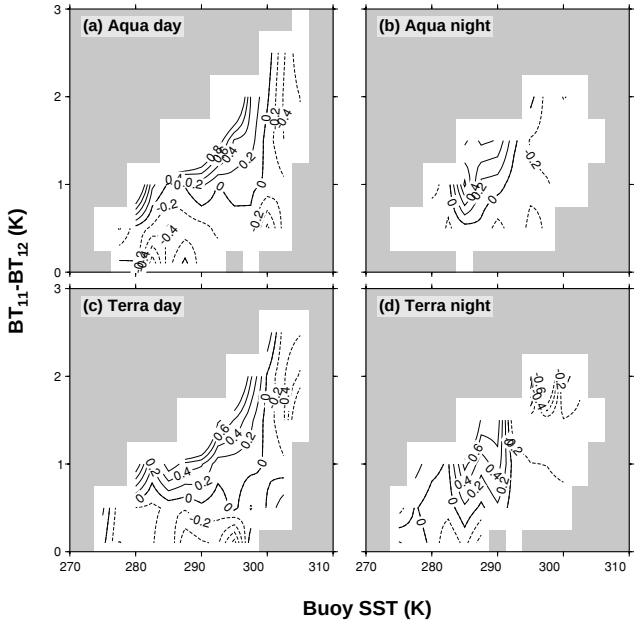

Fig. 8. Mean of MODIS SST errors on the domain of buoy SST and brightness temperature difference (BTD) between 11 mm and 12 mm bands. MODIS SST data are estimated using new MCSST algorithm. Means are calculated for every 0.5 K (BTD) by 2.5 K (buoy SST) box. Contour interval is 0.2 K. Solid/dashed lines indicate positive/negative errors, respectively. Shaded region indicates box with fewer than 20 observations.

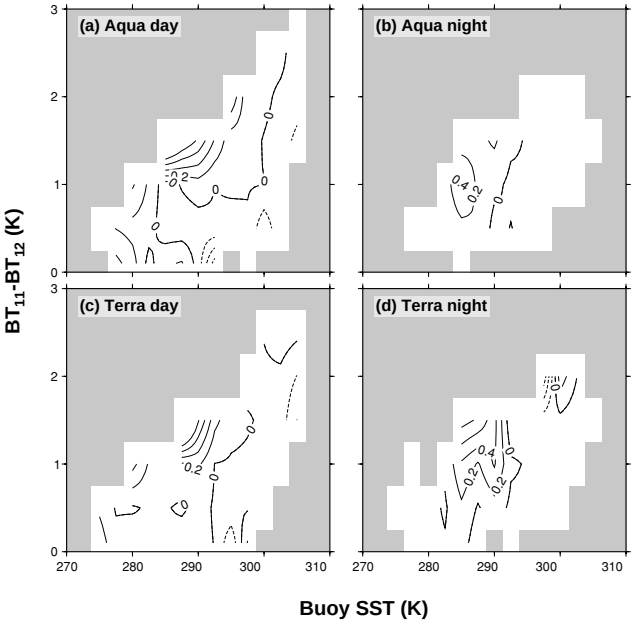

Fig. 9. Same as Fig. 8, except for the NLSST-3 algorithm.

of the NLSST-3 model also have such fluctuations, the amplitudes of biases are as small as 0.2 K and temporal variations of RMSE are suppressed.

The seasonal cycle and the biases related to true SST found in the results of MCSST model are explainable by nonlinear effects of water vapor in the atmosphere. Figure 8 shows the mean of MODIS MCSST errors (MODIS SST minus buoy SST) on the domain of sea-truth and BTD between 11 μm and 12 μm bands. In the MCSST algorithm, it is assumed that the BTD is linearly proportional to the water vapor. However, the errors of MODIS SST at an equivalent BTDs relate to the buoy SST values. The errors of MODIS SST are positive at middle and low SST ranges (SST < 290 K) and negative in the high SST range (SST > 290 K), if the BTDs are larger than 1 K. For nighttime estimation, when the near-infrared band is used, these features are weak but visible. Based on the fact that the negative errors means under-correction, under the same BTD condition, water vapor attenuation would be stronger over high SST regions than over a low SST region, as suggested by Fig. 8. The regions with SST higher

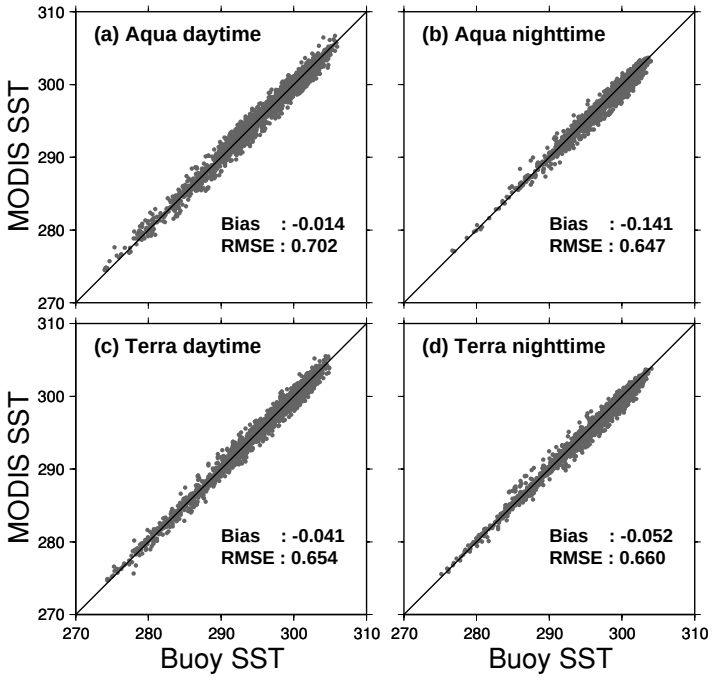

Fig. 10. Scatter diagrams of MODIS (NLSST-3) and buoy SST.

than 290 K spreads in summer: the bias of MODIS SST therefore reflects a seasonal cycle. The features can be reduced by the implementation of first-guess SST (T_{sfc}) in the regression equation (Eq. (6)), which is shown in Fig. 9. As it turns out, the seasonal variations of quality are depressed in NLSST.

5. Discussion

The quality of most nonlinear algorithms is superior to that of the MCSST algorithm. The temperature dependency and seasonal variability of the NLSST are weaker than those of the MCSST model. Although the WVSST model shows better quality than that of the NLSST model. Moreover, WVSST values in coastal regions are affected by land contamination in microwave observation. In addition, since simultaneous observations by the microwave radiometer are available only for Aqua, the WVSST model is not acceptable for near-real-time processing of the MODIS NRT SST. Although the QDSST models also have a quality comparable to that of the NLSST model, the bias depends on SST.

The SST values estimated from the MCSST model and Reynolds climatological data are unsuitable for a first-guess in the NLSST model, since RMSEs of estimated SST using these data are greater than those of the MCSST model in daytime. The low quality of the former is attributable to the noisy first-guess field, whereas that of the latter is probably the result of low spatial resolution. The first-guess SST in the NLSST model should be either Pathfinder climatological SST or near-real-time NGSST-O. The data quality using the two first-guess SST is similar. From the standpoint of reducing operational costs, Pathfinder data are desirable first-guess SSTs for near-real-time processing since it is not necessary to produce first-guess SST fields or to download them from other sites for pre-processing. Based on the results described here, the NLSST method using Pathfinder climatological data as a first-guess SST is used for the version 3 MODIS NRT SST algorithm processed at the JAXA/EORC. The MODIS estimation using the NLSST model with Pathfinder data as a first-guess SST plotted against the buoy-measured SST is shown in Fig. 10.

The diurnal variation of SST under cloud free conditions is made visible by using two MODIS observations (Terra, 10.30 AM; Aqua, 1:30 PM). We used the version 3 MODIS NRT SST, with sea surface wind (SSW) observed by AMSR-E aboard Aqua and daily mean solar downward flux (SDF) obtained from NCEP/NCAR reanalysis (Kistler *et al.*, 2001) as ancillary data. Figure 11 shows the mean SST variation in daytime around Japan in 2004. This result indicates the dependency of SST shift per hour from morning to afternoon on SSW and SDF, which is calculated from collocated data at a day observed by Terra and Aqua MODIS with their acquisition time in UTC. The SST is cooled in daytime if SDF is less than 120 W/m^2. From Tropical Rainfall Measuring

Mission (TRMM)/TRMM Imager (TMI) data, Gentemann *et al*. (2003) suggest that diurnal warming does not emerge when daily mean solar energy at the top of atmosphere is less than 132 W/m^2, which would concur with the result shown here. When the SSW is less than 6 m/s and the SDF is larger than 150 W/m^2, the SST variation per hour is greater than 0.1 K/hr. These characteristics of the SST diurnal correspond to the results based on one-dimensional model (Kawai and Kawamura, 2002) and satellite observation (Gentemann *et al*., 2003).

Donlon *et al*. (2002) pointed out that stratification in the upper-ocean layer during daytime are formed under low-wind conditions (SSW < 6 m/s). Satellite SST data collected by infrared sensors are estimated from the emitted radiation at a wavelength of 3.7–12 μm, at which the attenuation of radiation in water is at a depth of 10 μm. Since the buoy "bulk" SST data are measured within the upper 1 m layer of the ocean, it is possible that they do not coincide strictly with the satellite "skin" temperature. Figure 12 depicts a scatter diagram of SSW produced by AMSR-E and SST differences between Aqua/MODIS SST and buoy SST in daytime. The errors of SST have a positive bias with large standard deviation in the low-wind-speed regime, but they are slightly negative under high wind speeds. The match-up data used in this study are mostly observed under the middle-wind-speed state (SSW: 5–8 m/s). The coefficients developed for the version 3 MODIS NRT SST therefore correspond well to the buoy SST under the middle SSW condition, in which upper ocean stratification is not well formed. The regression influenced by the match-ups under the middle-wind-speed condition would cause positive errors in the low SSW regime, in which the skin temperature is higher than the bulk temperature. The influence of the errors under the low SSW condition worsens the quality of MODIS SST data. It might be useful to examine more closely some features of the influence of the surface stratification, by investigating the Aqua NLSST-3 (T_{sfc}: Pathfinder SST) algorithm. We developed the NLSST-3 algorithms with-

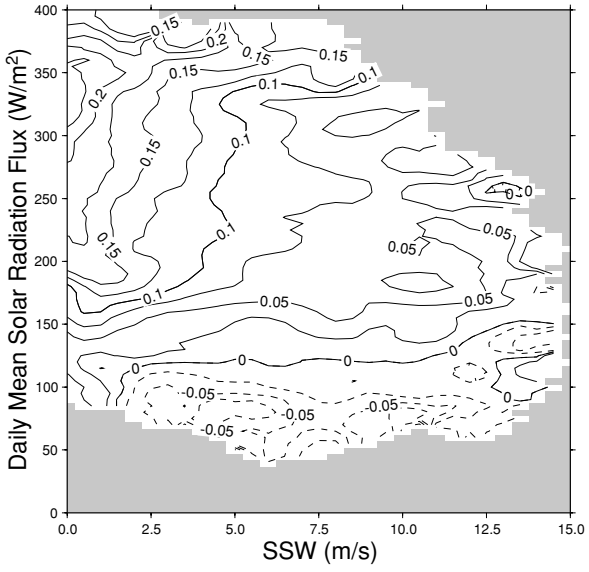

Fig. 11. Mean SST variation (K/hr) in daytime obtained from Terra/MODIS and Aqua MODIS, which is averaged in 0.5 m/s (SSW) by 5 W/m^2 box. Contour interval is 0.025 K/hr. Dashed lines indicate negative change; solid lines indicate positive. Shaded region signifies that the box containes fewer than 250 observations.

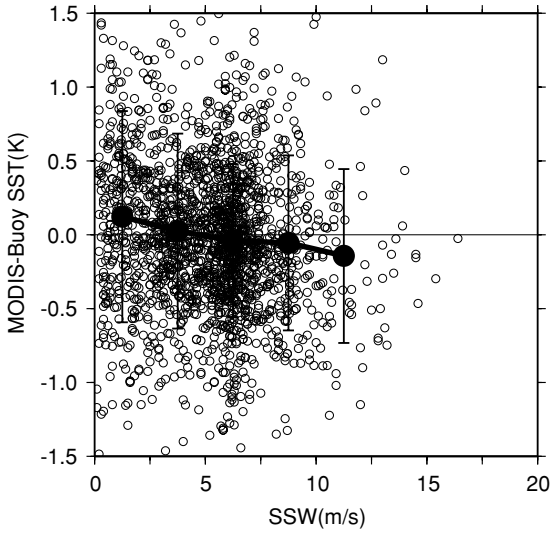

Fig. 12. Scatter diagram between SSW observed by AMSR-E and error of Aqua/MODIS SST (MODIS-buoy SST) in daytime. Solid line and error bar show the average and standard deviation of the error in every 2.5 m/s, respectively.

Table 5. RMSE of the Aqua MODIS NLSST-3 algorithms, which were developed for SSW greater than the threshold values.

SSW threshold (m/s)	0.0	0.1	2.0	3.0	4.0	5.0	6.0	7.0
Aqua MODIS (RMSE)								
Day	0.702	0.692	0.683	0.678	0.676	0.676	0.674	0.672
Night	0.647	0.646	0.649	0.645	0.648	0.648	0.644	0.642

out the match-ups under light-wind conditions and calculate the RMSE of each algorithms, as shown in Table 5. Although there is no apparent improvement in nighttime SST, the quality of MODIS SST in daytime is improved by the exclusion of observations under low wind speed conditions. The algorithms are not inproved further if the threshold value is larger than 3.0 m/s. Development of a retrieval algorithm of SST for a high-wind condition should be considered.

Atmospheric aerosol contamination is another cause of errors in satellite-derived SST. Smoke and dust aerosols are detected occasionally in the study area, especially in spring. Diaz *et al*. (2001) investigated the effects of atmospheric aerosols on satellite observation, concluding that the BTDs are sensitive to dust aerosols, but that no significant effect is exerted by smoke aerosols from biomass burning. Nalli and Stowe (2002) suggested an aerosol corrected SST algorithm for AVHRR using the reflectance ratio of two visible bands. Aerosol effects must be distinguished as between dust and aerosols, which can be accomplished using relatively new sensors such as MODIS and GLI. These issues should be addressed in future versions.

6. Summary

We have developed and validated MODIS near-real-time SST regional algorithms tuned to buoy-bulk SST observations in the western North Pacific region. Cloud detection algorithms were defined according to those for the ADEOS-II/GLI. Four atmospheric correction models were examined: MCSST, WVSST, QDSST, and NLSST. We have presented and examined four cases of a first-guess SST in NLSST models: values were estimated using the MCSST model, Reynolds or Pathfinder climatological SSTs, and near-real-time objective analysis data (NGSST-O). The coefficients for each model were derived from two-year match-up data and the models were validated against *in situ* observation for three years.

The qualities of MCSST and NLSST with MCSST are noisy, whereas land-contamination effects are found in WVSST model. Both MCSST and QDSST show biases related to true SST. The relation and seasonal cycles of bias and RMSE are suppressed in the NLSST model. A source of error in MCSST is the nonlinear effects of water vapor in the atmosphere on the BTDs. The spatial resolution of first-guess SST is inferred to be an important point in the NLSST method. From validation results, the NLSST model using Pathfinder SST as a first-guess SST is adopted as the version 3 MODIS NRT SST algorithm. The RMSEs of this new version MODIS NRT SST algorithm are reduced by 0.06–0.2 K from the version 2 algorithm.

Diurnal warmings in the study region calculated from two MODIS data observed in the morning (Terra) and early afternoon (Aqua) in the study region have been discussed using sea surface wind from AMSR-E and daily mean solar radiation flux from NCEP reanalysis. The ocean surfaces are cooled, even if the sea surface wind is weak, when the daily mean solar radiation flux is less than 120 W/m^2. The temporal variation of SST is noticeable if the solar radiation is larger than 150 W/m^2 and the sea surface wind is less than 6 m/s. The sources of error in estimating SST, including the surface stratification and aerosol contamination, have been discussed. An experimental study shows that the quality of estimation can be improved by taking the sea surface wind into consideration during algorithm development. Future work should specifically address correction of these issues.

Acknowledgements

We are grateful to members of JAXA/EORC for their thoughtful comments on this manuscript. Comments from three anonymous reviewers were very helpful and greatly improved the manuscript. This study is supported by the ADEOS-II project of JAXA Japan, and Category 7 of MEXT PR2002 Project for Sustainable Coexistence of Human, Nature and the Earth and Special Coordination Fund for Promoting Science and Technology "New Generation SST" of MEXT, Japan.

References

Ackerman, S. A., K. Strabala, W. P. Menzel, R. A. Frey, C. C. Moeller, L. E. Gumley, B. A. Baum, C. Shaaf and G. Riggs (1997): Discriminating clear sky from cloud with MODIS algorithm theoretical basis document (MOD35). Eos ATBD web site, 125 pp.

Brown, O. B. and P. J. Minnett (1999): MODIS infrared sea surface temperature algorithm, Algorithm Theoretical Basis Document (ATBD) Version 2.0. ATBD-MOD-25. Online document available at: http://modis.gsfc.nasa.gov/data/atbd/ocean_atbd.html

Diaz, J. P., M. Arbelo, F. J. Expósito, G. Podestá, J. M. Prospero and R. Evans (2001): Relationship between errors in AVHRR-derived sea surface temperature and the TOMS Aerosol Index. *Geophys. Res. Lett.*, **28**, 1989–1992.

Donlon, C. J., P. J. Minnett, C. Gentemann, T. J. Nightingale, I. J. Barton, B. Ward and M. J. Murray (2002): Toward improved validation of satellite sea surface skin temperature measurements for climate research. *J. Climate*, **15**, 353–369.

Emery, W. J., Y. Yu, G. A. Wick, P. Schluessel and R. W. Reynolds (1994): Correcting infrared satellite estimates of sea surface temperature for atmospheric water vapor attenuation. *J. Geophys. Res.*, **99**, 5219–5236.

Gentemann, C. L., C. J. Donlon, A. Stuart-Menteth and F. J. Wentz (2003): Diurnal signals in satellite sea surface temperature measurements. *Geophys. Res. Lett.*, **30**, doi:10.1029/2002GL016291.

Goodrum, G., K. B. Kidwell and W. Winston (2000): NOAA KLM User's guide—September 2000 revision. Technical

report. Online version http://ww2.nsdc.noaa.gov/docs/klm/
Guan, L., H. Kawamura and H. Murakami (2003): Retrieval of sea surface temperature from TRMM VIRS. *J. Oceanogr.*, **59**, 245–249.
Hosoda, K. (2004): Version up of MODIS near-real-time SST processing. On-line document available at: http://suzaku.eorc.jaxa.jp/GLI/ocean/modis_nrt/modis_sst_200409.pdf (in Japanese).
Kawai, Y. and H. Kawamura (2002): Evaluation of the diurnal warming of sea surface temperature using satellite-derived meteorological data. *J. Oceanogr.*, **58**, 805–814.
Kilpatrick, K. A., G. P. Podestá and R. Evans (2001): Overview of the NOAA/NASA advanced very high resolution radiometer Pathfinder algorithm for sea surface temperature and associated matchup database. *J. Geophys. Res.*, **101**, 9179–9197.
Kistler, R., E. Kalnay, W. Collins, S. Saha, G. White, J. Woollen, M. Chelliah, W. Ebisuzaki, M. Kanamitsu, V. Kousky, H. van den Dool, R. Jenne and M. Fiorino (2001): The NCEP-NCAR 50-year reanalysis: Monthly means CD-ROM and documentation. *Bull. Amer. Meteor. Soc.*, **77**, 437–471.
McClain, E. P., W. P. Pichel and C. C. Walton (1985): Comparative performance of AVHRR-based multichannel sea surface temperatures. *J. Geophys. Res.*, **90**, 11587–11601.
Murakami, H. (2002): Revision of near-real-time processing of MODIS SST at EORC. On-line document available at: http://suzaku.eorc.jaxa.jp/GLI/ocean/modis_nrt/MODISNRT_SSTrevision.pdf (in Japanese).
Nalli, N. R. and L. L. Stowe (2002): Aerosol correction for remotely sensed sea surface temperatures from national oceanic and atmospheric administration advanced very high resolution radiometer. *J. Geophys. Res.*, **207**, doi:10.1029/2001JC001162.
Reynolds, R. W. and T. M. Smith (1994): Improved global sea surface temperature analysis using optimum interpolation. *J. Climate*, **7**, 929–949.
Rossow, W. B. and L. C. Garder (1993): Cloud detection using satellite measurements of infrared and visible radiance for ISCCP. *J. Climate*, **6**, 2341–2369.
Sakaida, F. and H. Kawamura (1992): Estimation of sea surface temperature around Japan using the Advanced Very High Resolution Radiometer (AVHRR)/NOAA-11. *J. Oceanogr.*, **48**, 179–192.
Sakaida, F., M. Moriyama, H. Murakami, H. Oaku, Y. Mitomi, A. Mukaida and H. Kawamura (1998): The sea surface temperature product algorithm of the Ocean Color and Temperature Scanner (OCTS) and its accuracy. *J. Oceanogr.*, **54**, 437–442.
Sakaida, F., J.-I. Kudoh and H. Kawamura (2000): A-HIGHERS—The system to produce the high spatial resolution sea surface temperature maps of the western North Pacific using the AVHRR/NOAA. *J. Oceanogr.*, **56**, 707–716.
Sakaida, F., K. Hosoda, M. Moriyama, H. Murakami, A. Murakida and H. Kawamura (2006a): Sea surface temperature observation by Global Imager (GLI)/ADEOS-II: Algorithm and accuracy of the product. *J. Oceanogr.*, **62**, 311–319.
Sakaida, F., H. Kawamura, S. Takahashi, T. Shimada, Y. Kawai, K. Hosoda and L. Guan (2006b): Research and development of New Generation Sea Surface Temperature for open ocean (NGSST-O) and its demonstration operation. *J. Oceanogr.* (submitted).
Shenoi, S. C. (1999): On the suitability of global algorithms for the retrieval of SST from the north Indian Ocean using NOAA/AVHRR data. *Int. J. Remote Sensing*, **20**, 11–29.
Sobrino, J. A., Z.-L. Li and M. P. Stoll (1993): Impact of the atmospheric transmittance and total water vapor content in the algorithms for estimating satellite sea surface temperatures. *IEEE Trans. Geosci. Remote Sensing*, **31**, 946–952.
Stowe, L. L., P. Davis and E. P. McClain (1999): Scientific basis and initial evaluation of the CLAVR-1 global clear/cloud classification algorithm for the Advanced Very High Resolution Radiometer. *J. Atmos. Oceanic Technol.*, **16**, 656–681.
Strabala, K. I., S. A. Ackerman and W. P. Menzel (1994): Cloud properties inferred from 8–12-μm data. *J. App. Meteor.*, **33**, 212–229.
Tanahashi, S., H. Kawamura, T. Matsuura, T. Takahashi and H. Yusa (2000): Improved estimate of wide-ranging sea surface temperature from GMS S-VISSR data. *J. Oceanogr.*, **56**, 345–358.
Walton, C. C. (1988): Nonlinear multichannel algorithms for estimating sea surface temperature with AVHRR satellite data. *J. Appl. Meteorol.*, **27**, 115–124.
Walton, C. C., W. G. Pichel and J. F. Sapper (1998): The development and operational application of nonlinear algorithms for the measurements of sea surface temperatures with the NOAA polar-orbiting environmental satellites. *J. Geophys. Res.*, **103**, 27999–28012.
Wan, Z. (2002): Estimate of noise and systematic error in early thermal infrared data of the Moderate Resolution Imaging Spectroradiometer (MODIS). *Remote Sens. Env.*, **80**, 47–54.